https://dx.doi.org/10.22161/ijaers.710.11 ISSN: 2349-6495(P) | 2456-1908(O)

Study on the effect of ferrite number on impact toughness of austenitic stainless steels at low temperatures

André de Albuquerque Vicente[1], Peter Aloysius D'silva[1], Bobby Jos[1], Tiago Felipe de Abreu Santos[2], Jorge Alberto Soares Tenório[3]

[1]ESAB Middle East & Africa,Plot No. S20134, Jebel Ali Free Zone (South), PO Box 8964, Dubai, United Arab Emirates;
[2]Department of Mechanical Engineering, Universidade Federal de Pernambuco, Av. da Arquitetura, s/n, Cidade Universitária, Recife, PE, Brazil;
[3]Department of Chemical Engineering, Universidade de São Paulo, Rua do Lago,250, Cidade Universitária, São Paulo, SP, Brazil.

Abstract *— All ferrous materials, except the austenitic grades, exhibit a transition from ductile to brittle when tested above and below a certain temperature, called as ductile to brittle transition temperature (DBTT). In order to better understanding the effect of the volume fraction of δ ferrite in the impact toughness of austenitic stainless steels at low temperatures, the microstructures of welded joints of austenitic stainless steel produced through SAW, were studied. The groove welds were produced using welding electrodes and flux of the same specification, ER 316L 3.2 mm and a fluoride basic flux (CaF_2-Al_2O_3-SiO_2). The filler metals used are from different heats with different chemical compositions resulting in different ferrite numbers. The base metal used is AISI 316L TYPE plates of 25 mm thickness. The chemical compositions and the variation of the volume fractions of δ ferrite in the deposits were measured.The welded coupons were tested at -196 °C to measure the impact toughness. The results confirm that the volume fraction of δ ferrite is of paramount importance in the impact toughness of austenitic stainless steels at cryogenic temperatures. Complementary techniques of microstructural analysis were used, such as optical emission spectrometry, optical microscopy and quantitative image analysis.*

Keywords *— **Austenitic Stainless Steels; Impact Toughness; Ferrite Number; Cryogenics; DBTT.***

I. INTRODUCTION

The ductileto brittle transition temperature (DBTT) is a phenomenon that is widely observed in metals.Below critical temperature (DBTT), the material suddenly loss ductility and becomes brittle.

All ferrous materials (except the austenitic grades) exhibit a transition from ductile to brittle when tested above and below a certain temperature, called as ductileto brittle transition temperature.

The ductile to brittle transition behavior of a wide range of metals falls into three categories determined by their yield strength and crystal structure. Metals with a face centered cubic (FCC) crystal structure do not undergo the transition and retain their ductility at low temperature. This is because FCC metals present large number of slip systems in their crystal structure which allow dislocation slip to occur, even at very low temperature. Aluminum is an FCC metal and, therefore, does not become brittle at low temperature. Most hexagonal close packed metals (HCP), including magnesium and α titanium alloys, also do not undergo the transition effect. Metals with a body centered cubic (BCC) crystal structure often display ductile to brittle transition properties. Fracture in many BCC metals occurs by brittle cleavage at low temperatures and by ductile tearing at high temperature. **[1]**

https://dx.doi.org/10.22161/ijaers.710.11 ISSN: 2349-6495(P) | 2456-1908(O)

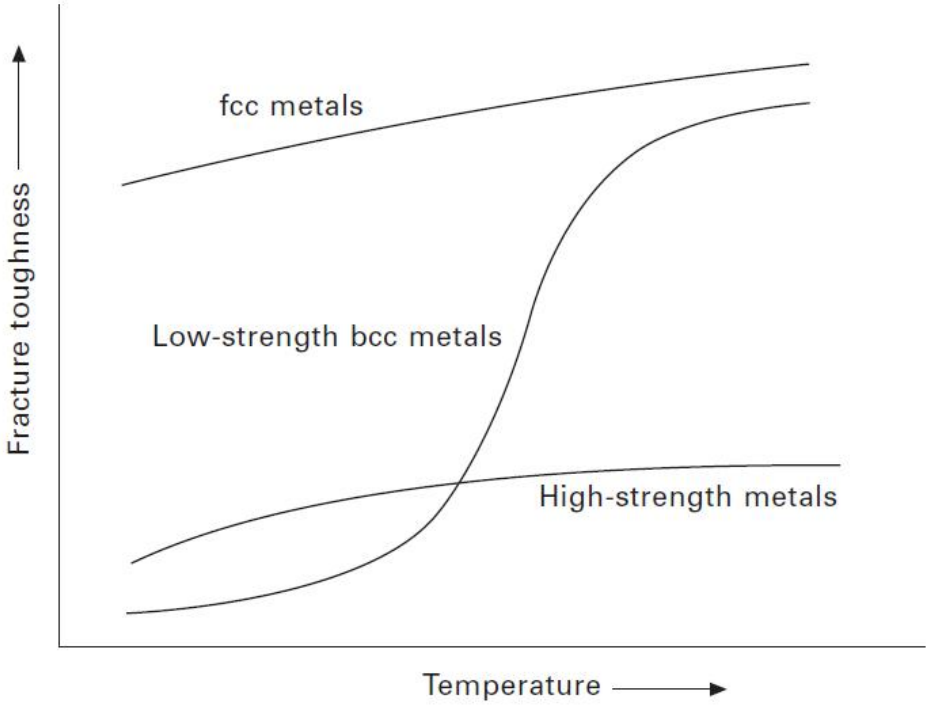

Fig.1: General trends of the ductile to brittle transition effect for different groups of metals. [1]

The ductile to brittle transition effect occurs because the development of the plastic zone in some types of metals is a temperature dependent process. At high temperatures, there is enough thermal energy in the crystal structure to aid the movement of dislocations under an externally applied stress. This allows the plastic zone to develop at the crack tip which then allows cracking to proceed by ductile fracture. The thermal energy to assist dislocation slip drops with temperature, and this makes it harder to develop the plastic zone. Dislocation mobility and, hence, the size of the plastic zone decrease rapidly below the transition temperature which results in a large loss in fracture toughness. Dislocation slip virtually stops below the transition temperature, which causes the metal to fracture by brittle crack growth.As temperature increases, the atoms in the material vibrate with greater frequency and amplitude. This increased vibration allows the atoms under stress to slip to new places in the crystal, break bonds and form new ones with other atoms. This slippage of atoms is seen on the outside of the material as plastic deformation, a common feature of ductile fracture. When temperature decreases however, the exact opposite is true. Atom vibration decreases, and the atoms do not want to slip to new locations in the material. When the stress on the material becomes high enough, the atoms just break their bonds and do not form new ones. This decrease in slippage causes little plastic deformation before fracture. Thus, a brittle type fracture takes place.**[1,2]**

The higher the dislocations density, the more brittle the fracture will be in the material. As dislocations density increases in a material due to stresses above the materials yield point, it becomes increasingly difficult for the dislocations to move because they pile into each other. It is important to emphasize that as grains get smaller, the fracture becomes more brittle,once that in smaller grains dislocations have less space to move before they hit a grain boundary. **[2]**

In welding of high alloy steels, the δ ferrite content is normally estimated from the constitution diagrams such as the Schaeffler**[3]**, DeLong **[4]** and Kotechi **[5]**.

In these diagrams, the δ ferrite contents of various welds had been measured experimentally by either metallography (Schaeffler) or magnetic methods (DeLong and WRC–92).**[6]**

The WRC – 92 diagram estimates the ferrite content to reasonably good accuracy, providing additional information about the solidification mode as shown on figure 2.

https://dx.doi.org/10.22161/ijaers.710.11 *ISSN: 2349-6495(P) | 2456-1908(O)*

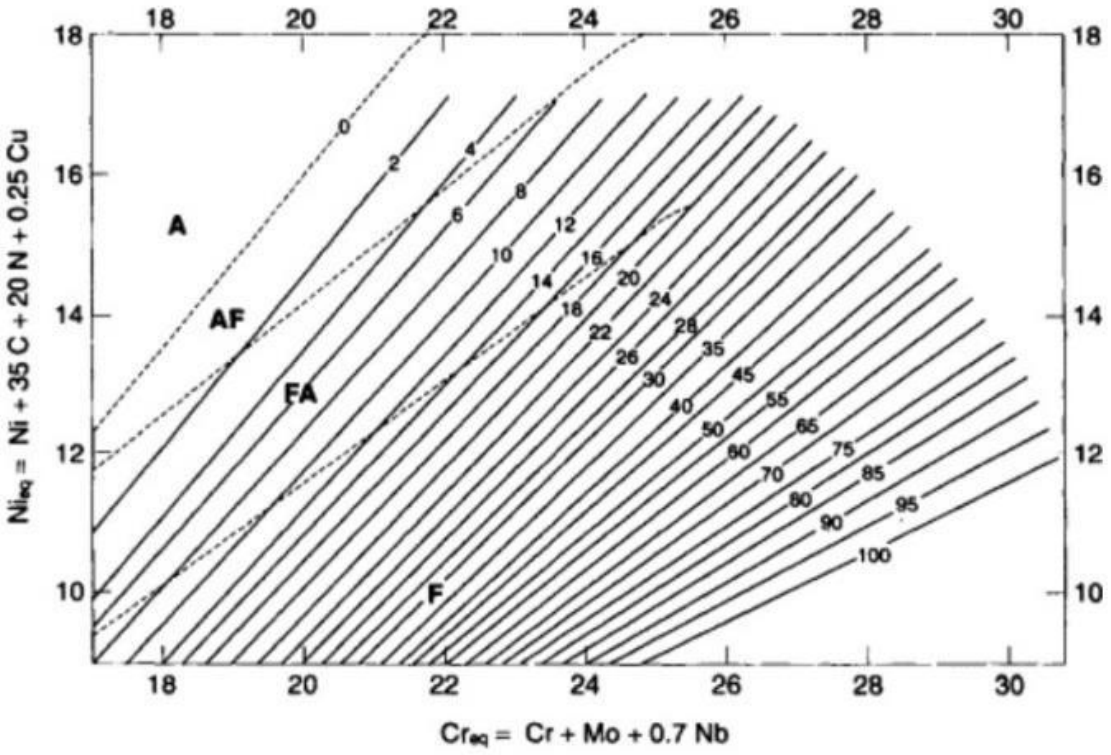

Fig.2: WRC-92 Diagram.[5]

Kotechi **[5]** has pointed out that there are number of alloying elements that have not been considered in the most accurate diagram to date, the WRC – 92 Diagram. Chemical elements like silicon, titanium and tungsten are not given due considerations though they are known to influence the ferrite content. He also stressed the point that cooling rate effects need to be considered more thoroughly in these constitution diagrams. **[6]**

Table 1 shows the expressions of chromium and nickel equivalents proposed by Schaeffler **[3]**, DeLong **[4]** and Kotechi **[5]**.

Table 1 - Cr_{eq} and Ni_{eq} formulae used for estimating the delta-ferrite content from constitution diagrams[6-8]

Consitution Diagram	
Schaeffler Diagram (1949)	Cr_{eq} = Cr + Mo + 1.5xSi + 0.5xNb
	Ni_{eq} = Ni + 30xC + 0.5xMn
DeLong Diagram (1973)	Cr_{eq} = Cr + Mo + 1.5xSi + 0.5xNb
	Ni_{eq} = Ni + 30xC + 30xN + 0.5xMn
WRC-92 Diagram (1992)	Cr_{eq} = Cr + Mo + 0.7xNb
	Ni_{eq} = Ni + 35xC + 20xN + 0.25xCu

When the Cr_{eq}/Ni_{eq} ratio < 1.5, the solidification may be austenitic (mode I) or austenitic-ferritic (mode II). When the ratio 1.5 < Cr_{eq}/Ni_{eq}< 2.0 the solidification will be ferritic-austenitic (mode III). And finally, when Cr_{eq}/Ni_{eq} ratio > 2.0 the solidification will be ferritic (mode IV). **[7-11]**

The possible solidification modes in the Fe-Cr-Ni system are:

I) ***Austenitic solidification ($L \rightarrow L+\gamma \rightarrow \gamma$):***

The only solid phase to form is austenite. In austenitic solidification, called solidification

https://dx.doi.org/10.22161/ijaers.710.11 *ISSN: 2349-6495(P) | 2456-1908(O)*

mode I, there is no other phase transformation at high temperature. **[7-8]**

II) **Austenitic-ferritic solidification *(L → L+γ→ L+γ+δ→γ+δ):***

Austenite solidifies as a primary phase in a dendritic or cellular way. As the temperature decreases, ferrite δ is formed from the remaining liquid. Solidification occurs through a peritectic reaction (L+δ→γ). This is called solidification mode II. **[7-11]**

III) ***Ferritic-austenitic solidification (L→L+δ→L+δ+γ→δ+γ):***

The duplex stainless steels solidify according to ferritic-austenitic solidification (L→L+δ→L+δ+γ→δ+γ). δ ferrite solidifies as the primary phase in dendritic or cellular fashion. As temperature decreases, austenite is formed by a peritectic (L+δ→γ) or eutectic (L→δ+γ) reaction. In the case of a peritectic reaction, the initially formed austenite completely surrounds the ferrite and subsequently grows into ferrite and liquid. Depending on the rate of diffusion through the austenite, the reaction may or may not be complete, and at the end of the solidification ferrite may be involved in austenite. Between the two reactions - peritectic and eutectic - the transition takes place where, during the initial formation of austenite by peritectic reaction, ferritizing elements secrete to the liquid, provoking their enrichment in these elements and consequently the simultaneous formation of ferrite and austenite by means of a eutectic reaction. This is called solidification mode III. **[7-17]**

IV) ***Ferritic solidification (L→L+δ→δ):***

The only solid phase to form is ferrite. In ferritic solidification, called solidification mode IV, ferrite is the only phase to form during solidification and, depending on the chemical composition, austenite can precipitate only in the solid state in the ferritic grain boundaries. **[7,8]**

The solidifications of austenitic stainless steels can occur according to the first three solidification modes. All ferrous alloys, except the austenitic grades, exhibit a transition from ductile to brittle temperature.

Unlike the austenite matrix, the δ ferrite presents a DBTT.This phase will be brittle at cryogenics temperatures and, depending on the volume fraction, will lead to embrittlement of the grain boundaries of the austenitic matrix.

As discussed before, it is reasonable to conclude that the volume fraction of δ ferrite is of paramount importance in the impact toughness of austenitic stainless steels at cryogenic temperatures.

II. EXPERIMENTAL

Two welded joints of austenitic stainless steel produced by the SAW process with different welding were studied. The groove welds were produced using welding electrodes and flux of the same specification, ER 316L 3.2 mm according to AWS 5.9, and a fluoride basic flux (CaF_2-Al_2O_3-SiO_2). The filler metals used are from different heats with different chemical compositions resulting in different ferrite numbers. The base metal used isAISI 316L TYPE plates of 25 mm thickness. The welding parameters used were the same in order to guarantee similar heat inputs for both joints.Afterwards, the samples were cut using a cut-off. Chemical analyzes were carried out in both samples at the face, middle and root of the all weld metals, by means of an optical emission spectrometer, according to ASTM E 1086-08. **[18]**

Transversal and longitudinal samples were embedded in hot-cure resin (bakelite). The conventional manual polishing was applied using water sandpapers (100, 240, 320, 400, 600 and 1000 mesh) in order to standardize the surface finish of the samples. A cloth polishing with 9, 3 and 1 μm diamond abrasive paste was carried out in this sequence. The samples were electrolytically attacked in 20% NaOH solution, 6V, for 90 seconds. This allowed the microstructural characterization of the samples through optical microscopy. The quantitative metallographic analysis for the determination of volumetric fractions of δ ferrite and austenite were performed according to ASTM E 562 ed. 08, **[19]** using a 4X5 grid (20 points) with a magnification of 400X in 30 different regions per test piece.Finally, impact toughness tests were performed on welded joints at -196 °C using Charpy impacttesting per ASTM E23-18. **[20]**.

III. RESULTS AND DISCUSSION

Table 2 presents the welding parameters used to weld the samples.It is important to emphasize that the welding wires used to produce samples 1 and2 were boththe ER316L according to AWS 5.9, 3.2 mm diameter, from different heats.

https://dx.doi.org/10.22161/ijaers.710.11 *ISSN: 2349-6495(P) | 2456-1908(O)*

Table 2–Welding parameters.

	Flux	Current (A)	Tension (V)	Driving Speed (mm/min)	Heat Input (kJ/mm)
Sample 1	CaF_2-Al_2O_3-SiO_2	400	27	400	1,62
Sample 2	CaF_2-Al_2O_3-SiO_2	400	27	400	1,62

Table 3 presents the chemical compositions and the calculations of C_{eq}, according to O. Hammar and U. Svensson **[7-8, 21],** of the base metal, filler metals and the all weld metals of the two joints.

Table 3– Chemical compositions and the calculations of C_{eq},

	C	Si	Mn	P	S	Cr	Ni	Mo	Cu	N	Ceq
AISI 316L (BM)	0.024	0.42	1.62	0.040	0.010	18,00	12.05	2.67	0.06	0.060	**0.063**
ER316L (FM1)	0.011	0.40	1.60	0.020	0.013	18.60	12.20	2.50	0.17	0.046	**0.041**
ER316L (FM2)	0.012	0.48	1.84	0.015	0.010	18.20	11.60	2.60	0.05	0.046	**0.042**
Sample1 (AW)	0.018	0.41	1.76	0.022	0.008	18,00	11.50	2.30	0.09	0.053	**0.052**
Sample2 (AW)	0.020	0.49	2,00	0.017	0.006	17.90	10.93	2.39	0.03	0.050	**0.053**

The results presented on table 3, show that the welded joints present less Cr, Mo and Ni and more C, Si and Mn than the filler metals.

Figure 3 shows the contents of C, Si, Mn, Cr, Ni and Mo (% by weight) of the base metal, filler metals ER 316L and all weld metals.

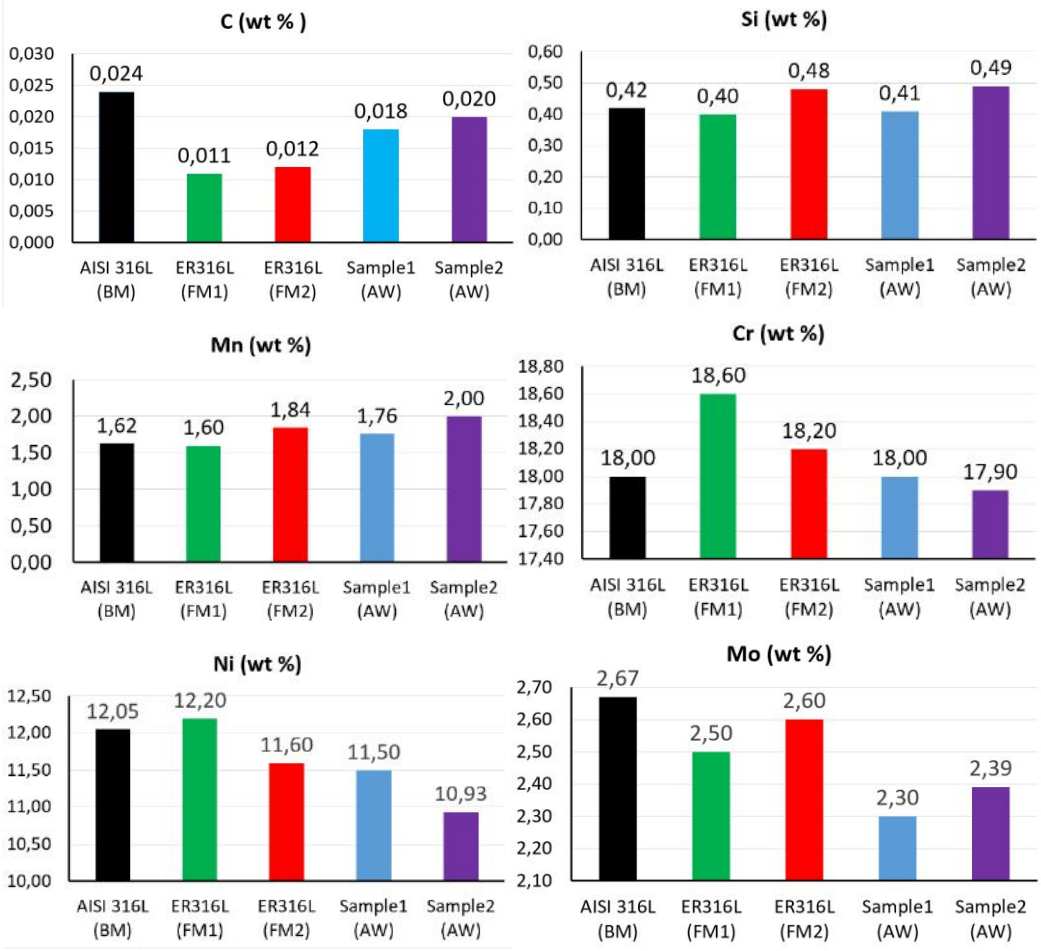

Fig.3: Contents of C, Si, Mn, Cr, Ni and Mo (% by weight) of the base metal, filler metals ER 316L and all weld metals.

https://dx.doi.org/10.22161/ijaers.710.11 *ISSN: 2349-6495(P) | 2456-1908(O)*

Table 4 presents calculated values ofCr_{eq}, Ni_{eq} and Cr_{eq}/Ni_{eq} ratio according to the expressions of chromium and nickel equivalents proposed by Schaeffler**[3]**, DeLong **[4]** and Kotechi **[5]**. The calculations of Cr_{eq}, Ni_{eq} and Cr_{eq}/Ni_{eq} ratio were done using formulas taken from Table 1.

Table 4– Cr_{eq}, Ni_{eq} and Cr_{eq}/Ni_{eq} ratio according to the expressions of chromium and nickel equivalents proposed by Schaeffler, DeLongand Kotechi.

	Schaeffler Diagram (1949)			**DeLong Diagram (1973)**			**WRC-92 Diagram (1992)**		
	Cr_{eq}	**Ni_{eq}**	**Cr_{eq}/Ni_{eq}**	**Cr_{eq}**	**Ni_{eq}**	**Cr_{eq}/Ni_{eq}**	**Cr_{eq}**	**Ni_{eq}**	**Cr_{eq}/Ni_{eq}**
AISI 316L (BM)	21.30	13.58	**1.57**	21.30	15.38	**1.38**	20.67	14.11	**1.46**
ER316L (FM1)	21.70	13.33	**1.63**	21.70	14.71	**1.48**	21.1	13.55	**1.56**
ER316L (FM2)	21.52	12.88	**1.67**	21.52	14.26	**1.51**	20.8	12.95	**1.61**
Sample1 (AW)	20.92	12.92	**1.62**	20.92	14.51	**1.44**	20.3	13.21	**1.54**
Sample2 (AW)	21.03	12.53	**1.68**	21.03	14.03	**1.50**	20.29	12.64	**1.61**

Figure 4 shows the variations of the Cr_{eq} and Ni_{eq} values (% by weight) of the base metal, filler metals ER 316L and all weld metals.

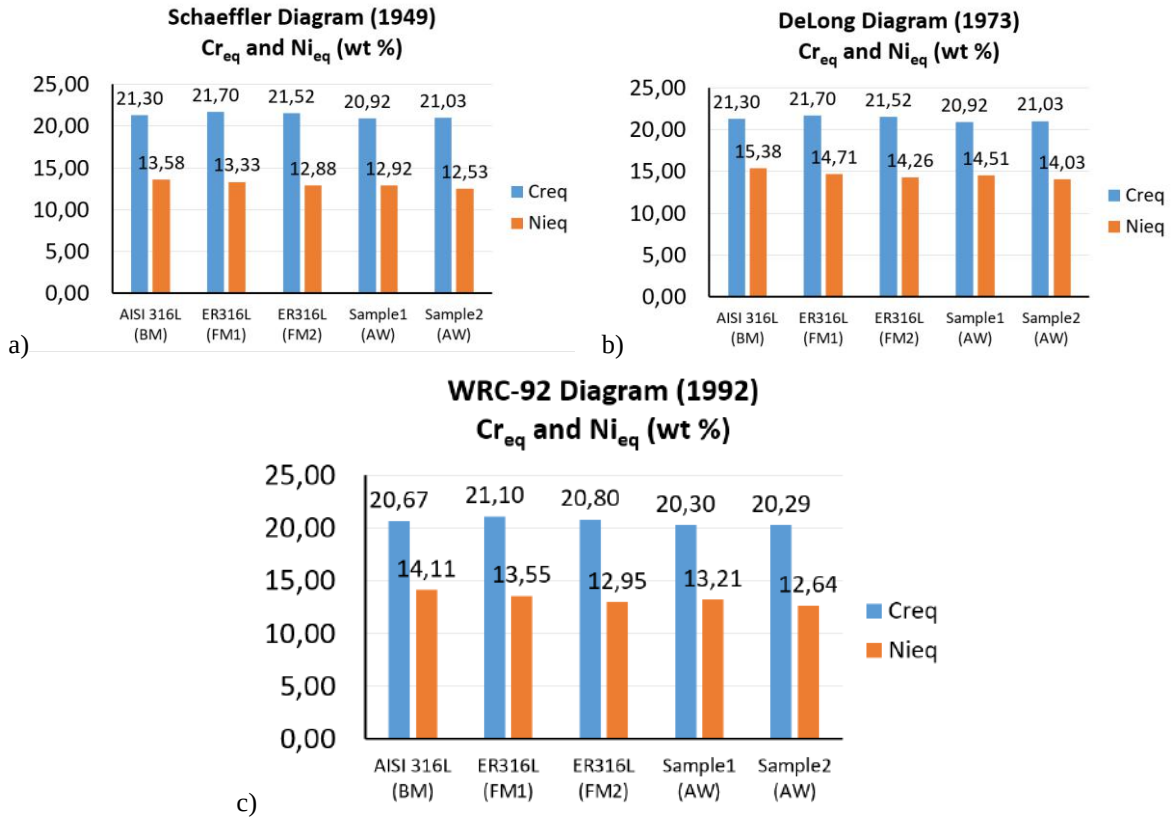

Fig.4: Cr_{eq} and Ni_{eq} values (% by weight) of the base metal, filler metals ER 316L and all weld metals, according to the expressions of chromium and nickel equivalents proposed by:
a) Schaeffler, b) DeLongand c) Kotechi.

https://dx.doi.org/10.22161/ijaers.710.11 *ISSN: 2349-6495(P) | 2456-1908(O)*

Figure 5 shows the variations of the Cr_{eq}/Ni_{eq} ratio of the base metal, filler metals ER 316L and all weld metals.

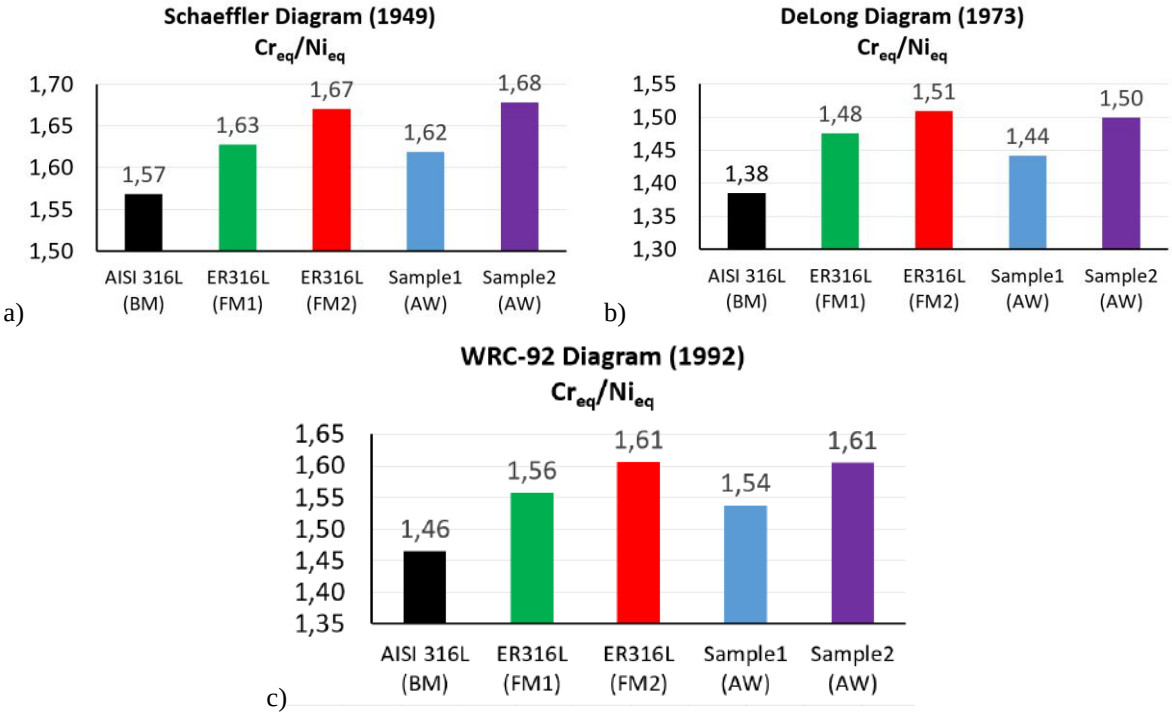

Fig.5: Cr_{eq}/Ni_{eq} ratio of the base metal, filler metals ER 316L and all weld metals, according to the expressions of chromium and nickel equivalents proposed by:a) Schaeffler, b) DeLongand c) Kotechi.

Table 5 presents the volume fractions of δ ferrite measured through metallographic analysis in 30 different regions per test piece.

Table 5– Volume fractions of δ ferrite measured through optical microscopy.

Volume fraction of δ ferrite	Mean	95%CI	%RA
AISI 316L (BM) Transversal	6.1	1.7	11.2
AISI 316L (BM)Longitudinal	3.7	1.9	14.1
AISI 316L (BM)- Average	**4.6**	**2.0**	**9.6**
Sample 1 (AW) Transversal	7.3	1.5	12.1
Sample 1 (AW)Longitudinal	4.3	1.7	9.6
Sample 1 (AW)- Average	**5.4**	**1.9**	**10.1**
Sample 2 (AW)Transversal	9.0	1.7	14.2
Sample 2 (AW)Longitudinal	6.3	1.7	10.1
Sample 2 (AW)- Average	**7.3**	**1.8**	**11.1**

Metallographic analysis revealed a solid austenitic-ferritic microstructure of solidification for all welded specimens, with austenite being the light phase and ferrite being the dark phase in the grain boundaries.The volumetric fractions of δ ferrite verified in the longitudinal direction are smaller than those verified for the transversal direction in the four welded specimens.

Figure 6shows the plots of the chemical compositions of the base metal, filler metals ER 316L and all weld metals, on the constitution diagrams proposed by Schaeffler**[3]**, DeLong **[4]** and Kotechi **[5]**.

https://dx.doi.org/10.22161/ijaers.710.11 *ISSN: 2349-6495(P) | 2456-1908(O)*

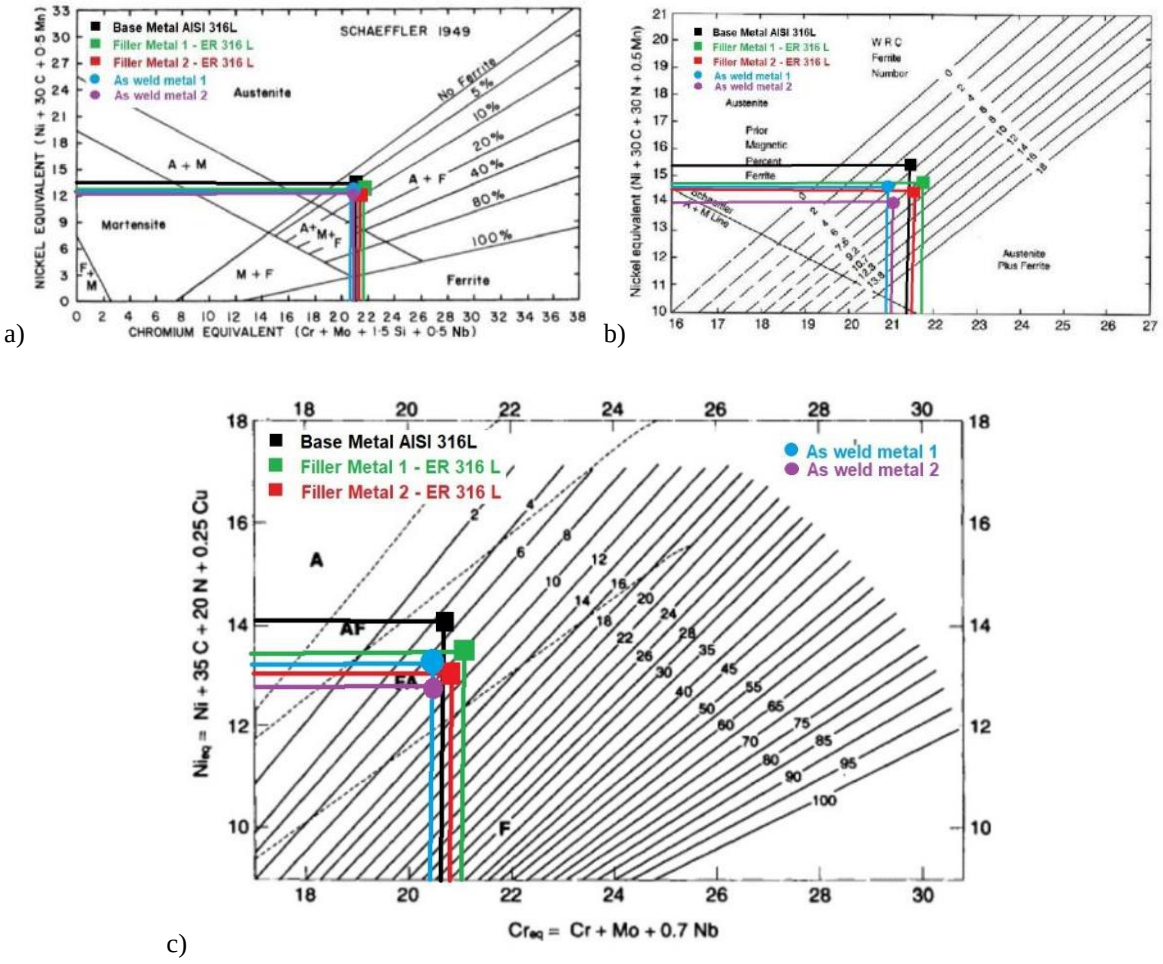

Fig.6: Plots of the chemical compositions of the base metal, filler metals ER 316L and all weld metals, on the constitution diagrams proposed by:a) Schaeffler, b) DeLong and c) Kotechi.

Table 6 presents the results of the impact toughness tests performed on welded joints at -196 °C using Charpy impacttesting.

Table 6– Impact toughness tests performed on welded joints at -196 °C using Charpy impact testing.

	Energy Absorbed (J)					
	CVN1	**CVN2**	**CVN3**	**CVN4**	**CVN5**	**Mean**
Sample1 (AW)	42	47	40	47	41	**43**
Sample2 (AW)	24	24	22	24	22	**23**
	Lateral Expansion (mm)					
	CVN1	**CVN2**	**CVN3**	**CVN4**	**CVN5**	**Mean**
Sample1 (AW)	0.62	0.61	0.56	0.51	0.55	**0.57**
Sample2 (AW)	0.45	0.48	0.41	0.39	0.38	**0.42**

As discussed earlier, the results confirm that the volume fraction of δ ferrite is of paramount importance in the impact toughness of austenitic stainless steels at cryogenic temperatures.

IV. CONCLUSIONS

The ferrite number of the joint is directly linked to the ferrite number of the filler metal.The welded joints produced using

https://dx.doi.org/10.22161/ijaers.710.11 *ISSN: 2349-6495(P) | 2456-1908(O)*

the filler metal with higher ferrite number, presented higher ferrite number and vice versa.

Although the variations of Cr_{eq} and Ni_{eq}, both welded joints presented the same ferritic-austenitic solidification mode (mode III).

The chemical results of the welded joints suggest that the welding of austenitic stainless steels using SAW process is very sensitive to the flux. Using a flux of the type CaF_2-Al_2O_3-SiO_2 resulted in decrease of Cr, Mo and Ni and increase of C, Si and Mn contents in the all weld metal when compared with the chemical compositions of the filler metals.

The results obtained confirm that the volume fraction of δ ferrite is of paramount importance in the impact toughness of austenitic stainless steels at cryogenic temperatures.

The joint that presented lower ferrite number, presented better performance in the impact toughness of austenitic stainless steels at cryogenic temperatures.

REFERENCES

[1] Mouritz, A. P.. "Fracture toughness properties of aerospace materials", in: Introduction to Aerospace Materials. Woodhead Publishing, 2012, Pages 454-468, ISBN 9781855739468, https://doi.org/10.1533/9780857095152.454.

[2] Pineau, A.. "Practical Application of Local Approach Methods", in: Comprehensive Structural Integrity. Editor(s): I. Milne, R.O. Ritchie, B. Karihaloo, Pergamon, 2003, Pages 177-225, ISBN 9780080437491, https://doi.org/10.1016/B0-08-043749-4/07096-8.

[3] SCHAEFFLER, A. L.. **Constitution diagram for stainless steel weld metal**. Metal Progress, vol. 56, n.5, p. 680-680B, 1949.

[4] DeLONG, W. T.. **A modified phase diagram for stainless steel weld metals.**Metal Progress, p. 98-100B, 1960.

[5] D.J. KOTECHI; D. T. A. SIEWERT. **WRC – 92 Constitution Diagram for Stainless Steel Weld Metals: a Modification of the WRC – 1988 Diagram**. Welding Journal 71 (5), 171–178, 1992.

[6] M. Vasudevan, M. Murugananth, A.K. Bhaduri, **Application of Bayesian neural network for modeling and prediction of FN in austenitic stainless steel welds**, in: H. Cerjak, H.K.D.H. Bhadeshia (Eds.), Mathematical Modelling of Weld Phenomena—VI, Institute of Materials, 2002, pp. 1079–1099.

[7] Vicente, A. A.. **Estudo da resistência à oxidação ao ar a altas temperaturas de um aço inoxidável austenítico microligado ao cério soldado pelo processo mig/mag com diferentes gases de proteção.** Tese de Doutorado, Escola Politécnica, Universidade de São Paulo, São Paulo. 2017. https://doi:10.11606/T.3.2017.tde-05092017-103140.

[8] VICENTE, A. A.; D'SILVA, P. A.; SANTOS, I. L.; AGUIAR, R. R.; JUNIOR, A. B. B;SANTOS, T. F. A..**The effect of shielding gases in the Ferrite Number of austenitic stainless steels joints through GMAW.** International Journal of Advanced Engineering Research and Science, 7(7), pp.332-341, 2020. https://doi.org/10.22161/ijaers.77.37.

[9] VICENTE, A. A.; D'SILVA, P. A.; SOUZA, R. L.; SANTOS, I. L.; AGUIAR, R. R.; JUNIOR, A. B. B..**The use of duplex stainless steel filler metals to avoid hot cracking in GTAW welding of austenitic stainless steel AISI 316L.** International Journal of Advanced Engineering Research and Science, 7(6), pp.345-355, 2020. https://doi.org/10.22161/ijaers.76.43.

[10] VICENTE, A. A.; SOUZA, R. L.; ESPINOSA, D. C. R.; AGUIAR, R. R.; PAUL, P.. **Effect of relative plate thickness in the heat flow and cooling rate during welding of super duplex stainless steel.** Saudi Journal of Engineering and Technology, 5 (5), 244-150. Scholars Middle East Publishers, Dubai, United Arab Emirates, 2020. https://doi.org/10.36348/sjet.2020.v05i05.005.

[11] VICENTE, A. A.; SANTOS, I. L.; JUNIOR, A. B. B.; ESPINOSA, D. C. R.; TENÓRIO, J. A. S.. **Study of the Distribution of Cr, Mo, Ni and N in δ Ferrite and Austenite in Duplex Stainless Steels**. Saudi Journal of Engineering and Technology, 5 (4), 156-162. Scholars Middle East Publishers, Dubai, United Arab Emirates, 2020. https://doi.org/10.36348/sjet.2020.v05i04.005.

[12] Santa-Cruz, L. A., Machado, G., Vicente, A. A. et al. **Effect of high anodic polarization on the passive layer properties of superduplex stainless steel friction stir welds at different chloride electrolyte pH values and temperatures.**Int J Miner Metall Mater 26, 710–721 (2019). https://doi.org/10.1007/s12613-019-1790-0.

[13] MARQUES, Igor Jordão; VICENTE, André de Albuquerque; TENORIO, Jorge Alberto Soares and SANTOS, Tiago Felipe de Abreu. **Double Kinetics of Intermetallic Phase Precipitation in UNS S32205 Duplex Stainless Steels Submitted to Isothermal Heat Treatment.** Materials Research, 20(Suppl. 2), 152-158. Epub June 26, 2017. https://doi.org/10.1590/1980-5373-mr-2016-1060.

[14] A. de Albuquerque Vicente, J.R.S. Moreno, D.C.R. Espinosa, T.F. de Abreu Santos, J.A.S. Tenório. **Study of the high temperature oxidation and Kirkendall porosity in dissimilar welding joints between FE-CR-AL alloy and stainless steel AISI 310 after isothermal heat treatment at 1150 °C in air.**J. Mater. Res. Technol. 8(2), 1636 (2019). https://doi.org/10.1016/j.jmrt.2018.11.009.

[15] Vicente, A. A.; Cabral, D. A.; Espinosa, D. C. R.; Tenório, J. A. S.. **Efeito dos gases de proteção na microestrutura e nas cinéticas de oxidação a altas temperaturas ao ar de juntas soldadas de um aço inoxidável austenítico através do processo MIG/MAG.** Tecnol. Metal. Mater. Min., vol.14, n4, p.357-365, 2017. https://doi.org/10.4322/2176-1523.1264.

[16] MARQUES, Igor Jordão; SILVA, Flavio J.; SANTOS, Tiago Felipe de Abreu. **Rapid precipitation of intermetallic phases during isothermal treatment of duplex stainless steel joints produced by friction stir**

https://dx.doi.org/10.22161/ijaers.710.11 *ISSN: 2349-6495(P) | 2456-1908(O)*

welding. Journal of Alloys and Compounds, Volume 820, 2020. https://doi.org/10.1016/j.jallcom.2019.153170.

[17] Santa Cruz, L. A., Marques, I. J., Urtiga Filho, S .L. et al. **Corrosion Evaluation of Duplex and Superduplex Stainless Steel Friction Stir Welds Using Potentiodynamic Measurements and Immersion Tests in Chloride Environments.** Metallogr. Microstruct. Anal. 8, 32–44 (2019). https://doi.org/10.1007/s13632-018-0506-6.

[18] ASTM E1086-08: Standard Test Method for Optical Emission Vacuum Spectrometric Analysis of Stainless Steel by the Point-to-Plane Excitation Technique. ASTM International. West Conshohocken. PA. EUA. 2008.

[19] ASTM E562-08: Standard Test Method for Determining Volume Fraction by Systematic Manual Point Count. ASTM International. West Conshohocken. PA. EUA. 2008.

[20] ASTM E23-18: Standard Test Methods for Notched Bar Impact Testing of Metallic Materials. ASTM International. West Conshohocken. PA. EUA. 2018.

[21] HAMMAR, O.; SVENSSON, U.. **Influence of Steel Composition on Segregation and Microstructure During Solidification of Austenitic Stainless Steels.** Solidification and Casting Metals, London, Metals Society, p. 401- 410, 1979.